Molecular Therapy
Nucleic Acids
Original Article

Splicing correction by peptide-conjugated morpholinos as a novel treatment for late-onset Pompe disease

Ryan A. Oliver,[1,2] Meghan E. Ahern,[1,3] Perla G. Castaneda,[1,3] Tushare Jinadasa,[1] Anirban Bardhan,[1] Kathy Y. Morgan,[1] Kristin Ha,[1] Kailash Adhikari,[1] Nino Jungels,[1] Noa Liberman,[1] Anindita Mitra,[1] Christopher D. Greer,[1] Alec M. Wright,[1] Emily G. Thompson,[1] Stephanie Garcia,[1] Elena Copson,[1] Senkara Allu,[1] Xuyu Tan,[1] Alex J. Callahan,[1] Bao Zhong Cai,[1] Vincent Guerlavais,[1] Kevin J. Kim,[1,2] and Annika B. Malmberg[1,2]

[1]Sarepta Therapeutics, Inc, 215 First Street, Cambridge, MA 02142, USA

Late-onset Pompe disease (LOPD) is overwhelmingly caused by a single mutation that disrupts splicing of acid-alpha glucosidase (*GAA*) and results in the accumulation of lysosomal glycogen in muscle cells leading to progressive muscle weakness in patients. Current therapeutics for LOPD do not meet the needs of patients and have largely been developed in mutant animal models lacking *Gaa* expression, which more closely mimic the less common infantile form of the disease. Here we design and evaluate peptide-conjugated phosphorodiamidate morpholino oligomers (PPMOs) to target the causative mutation in *GAA* and correct pathogenic splicing in muscle tissue. We show PPMO compounds correct LOPD splicing in both patient induced pluripotent stem cell-derived muscle cells and in skeletal muscle tissue after intravenous dosing in a newly developed humanized LOPD animal model that recapitulates patient LOPD splicing.

INTRODUCTION

Pompe disease (PD) is a muscle wasting disease broadly characterized by age of onset: infantile-onset PD (IOPD) is underscored by a severe phenotype with cardiac involvement from birth, while the late-onset PD (LOPD) affects mainly skeletal muscle and is characterized by a range of onset generally in the second decade of life.[1–3] As the current standard of care for PD, enzyme replacement therapy has proven beneficial for IOPD patients but offers fewer clinical benefits to LOPD patients in part due to its hampered ability to target skeletal muscle in addition to eliciting an immune response.[4–6]

LOPD is largely underscored by faulty splicing of acid-alpha glucosidase (*GAA*) caused by the single widespread IVS1 point mutation c.-32-13T>G (Figure 1A).[7,8] GAA is a lysosomal glycoside hydrolase responsible for the degradation of glycogen into glucose. Pathogenic GAA levels, therefore, lead to lysosomal accumulation of glycogen in the muscle cells of patients that results in defective autophagy and cell death.[5,9,10]

The majority of LOPD patients are compound heterozygous for mutations in *GAA*. Sixty-eight percent to 90% of LOPD patients carry the common IVS1 mutation.[11] The IVS1 mutation affects an estimated 1:30,000 individuals in the United States and disrupts splicing of *GAA* producing several nonproductive splice variants in which ATG-containing exon 2 is completely or partially skipped (Figures 1A and S1).[12–15] However, this mutation does not completely disrupt *GAA* splicing, instead allowing for 10%–15% residual canonical splicing.[16] The greatly attenuated exon 2 inclusion caused by the IVS1 mutation leads to the milder phenotype observed in LOPD compared with IOPD. Given that GAA-pseudodeficient carriers of PD are by definition unaffected, we hypothesized that precision genetic therapeutic rescue of the IVS1 mutant allele would greatly benefit LOPD patients.

Recently, significant progress has been made illuminating the underpinnings of the IVS1 mutation in *GAA*. It has been shown that the IVS1 mutation lies in the polypyrimidine tract of exon 2, thus interfering with splicing factor recognition of the downstream splice acceptor site.[17] Several naturally occurring transcript variants (TVs) of *GAA* are affected by the IVS1 mutation and misspliced in similar patterns to produce several pathological splice variants in which exon 2 is skipped (Figure S1). Additionally, data suggest that a pseudoexon contained inside intron 1 is activated in the presence of the IVS1 mutation.[16] The incorporation of this pseudoexon also contributes to faulty *GAA* splicing and subsequent pathological GAA levels. Further, steric active oligonucleotides have been shown to rescue the IVS1 splicing pathology but require delivery vehicles to elicit their effects.[16,18–20]

Received 9 July 2024; accepted 21 March 2025;
https://doi.org/10.1016/j.omtn.2025.102524.

[2]Senior author

[3]These authors contributed equally

Correspondence: Kathy Y. Morgan, Sarepta Therapeutics, Inc, 215 First Street, Cambridge, MA 02142, USA.
E-mail: katmorgan@sarepta.com

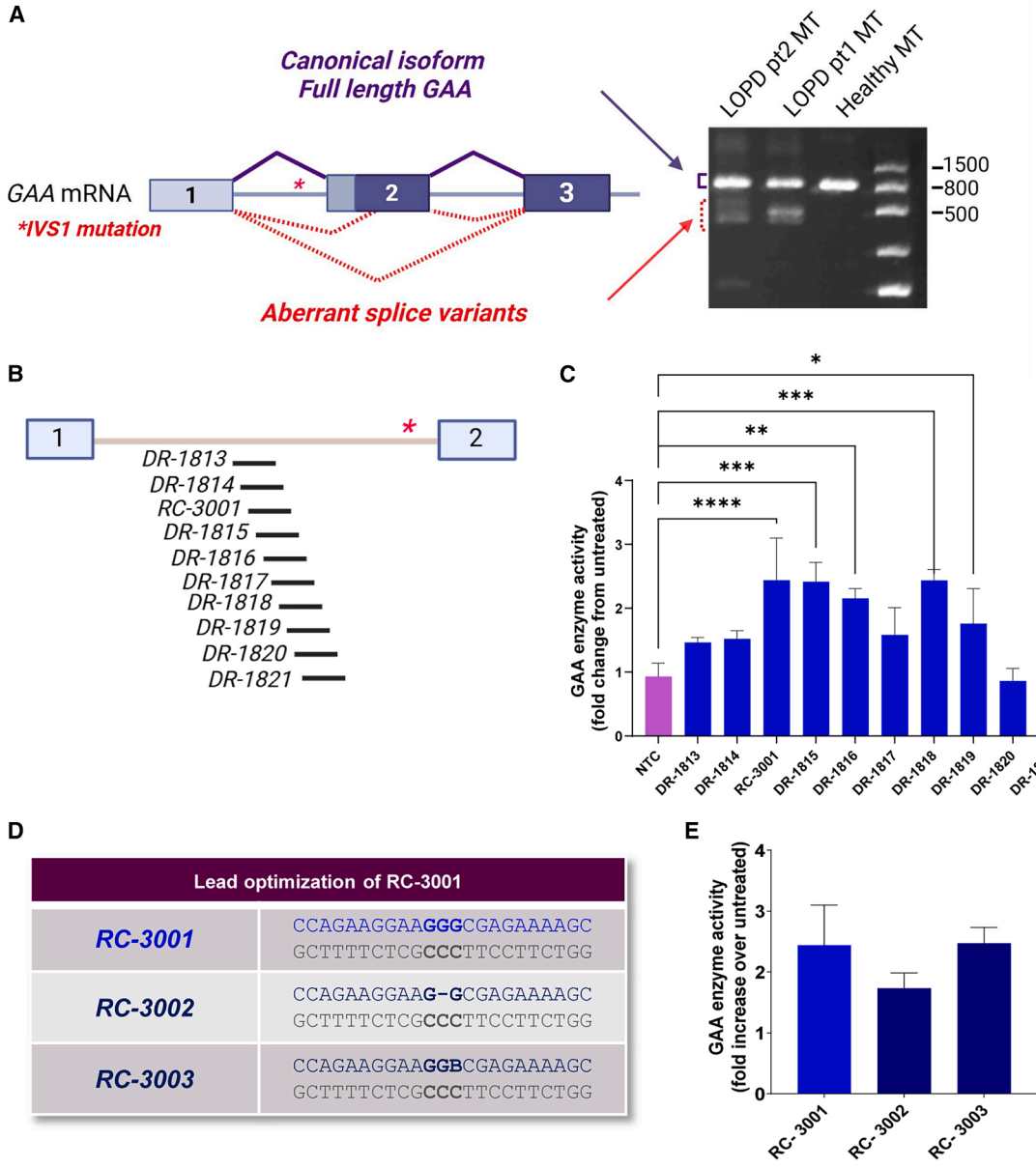

Figure 1. PPMO increases GAA enzyme activity in patient-derived fibroblasts

(A) *GAA* mis-splicing caused by the common IVS1 mutation (red) compared with canonical *GAA* splicing (black). Splicing events were detected by endpoint RT-PCR. (B) Schematic depicting the location of PPMO compounds in microwalk screen. (C) Members of the microwalk screen were assayed for increases in GAA enzyme activity in LOPD patient fibroblasts. NTC = nontargeting control. One-way ANOVA with Dunnett's multiple comparison test. *$p < 0.05$, **$p < 0.01$, ***$p < 0.001$, ****<0.0001. (D) Optimization of hit compound sequence RC-3001 using an abasic subunit to address high GC content. (E) Abasic-containing sequence (RC-3003) restores GAA enzyme activity in patient fibroblasts. Results are expressed as mean with error bars (SD).

Modulation of RNA splicing through the use of antisense oligomers has emerged as a powerful technology in the treatment of various human genetic diseases.[21] Through various chemical scaffolds, these compounds have been used to modulate gene expression through pre-mRNA splicing modulation, binding to key regulatory elements, and interactions with *trans*-acting RNA expression regulators.[21,22]

Here, we use peptide-conjugated phosphorodiamidate morpholino oligomers (PPMOs) to correct the pathogenic IVS1 splicing found in LOPD. First, we screened a targeted library of PPMOs for optimal GAA enzyme activity restoration in patient fibroblasts. Next, we generated a disease-relevant patient induced pluripotent stem cell (iPSC)-derived *in vitro* myotube model of LOPD to further validate the most active PPMO compounds. Finally, we generated a

humanized mouse model of LOPD that recapitulates the *GAA* mis-splicing found in patients and use this model to demonstrate target engagement and correction of pathogenic *GAA* splicing in skeletal muscle after intravenous (IV) treatment with PPMO compounds.

RESULTS

PPMOs increase GAA enzyme activity in patient-derived fibroblasts

We first designed a library of PPMO compounds that utilized the short polyarginine cell-penetrating peptide Ac-N-Arg_6-Gly-OH conjugated to a PMO sequence complementary to the human *GAA* intron 1 locus near the IVS1 mutation (Figure 1B; Table S1). PPMOs were screened in patient-derived fibroblasts by gymnotic uptake at 20 μM concentration, followed by analysis of lysosomal GAA enzyme activity in cellular lysates after 4 days of treatment (Figure 1C). Based on these results, we identified a number of compounds that increased GAA enzyme activity. The most active compound RC-3001 increased GAA enzyme activity by approximately 2.4-fold compared with a nontargeting control and was selected for further optimization. Analysis of RC-3001 by dynamic light scattering (DLS) (Figure S2) and size exclusion chromatography (SEC) (Figure S3) indicated the potential for significant aggregation, likely due to the string of guanine residues contained in the PPMO sequence (Figure 1D).[23,24] We therefore sought to mitigate the guanine repeat content of the sequence by removal of a guanine (RC-3002) or replacement of a guanine with an abasic subunit (RC-3003). In the case of guanine removal, aggregation as measured by DLS and SEC improved, but efficacy was reduced (Figures 1E, S2, S4, and S5). On the other hand, substitution of a single guanine residue with an abasic subunit (Figure 1D) significantly decreased cytotoxicity as measured by lactate dehydrogenase (LDH) assay (Figure S6) and further improved the aggregation profile while retaining full potency of the starting sequence (Figure 1E). Assessing the dose response relationship confirmed the restoration of efficacy using the abasic sequence (Figure S7A).

We further probed the efficacy of the abasic-containing RC-3003 in an additional patient fibroblast line and compared the GAA enzyme activity levels of treated and untreated patient fibroblasts to the average activity of two healthy fibroblast lines (Figure S7B). After a single 20 μM gymnotic concentration of RC-3003, GAA enzyme activity levels in both patient fibroblast lines increased from 8%–10% to 21%–25% of the healthy control lines. Based on these data, we selected RC-3003 for further evaluation.

LOPD patient-derived iPSC lines mimic splicing found in LOPD patients

Because LOPD primarily affects muscle tissue, we sought to validate the mechanism and efficacy of PPMO compounds in terminally differentiated skeletal muscle cells derived from patients. To this end, we reprogrammed two LOPD patient fibroblast lines to iPSCs using a feeder-free and footprint-free method (Figure S8). Pluripotency was validated by immunostaining with markers Oct3/4, NANOG, and TRA-1-60 (Figures 2A and S9). iPSCs retained normal karyotype and alkaline phosphatase activity (Figures S10 and S11). iPSC lines were differentiated to myoblasts, frozen, and revived. Myogenic lineage was confirmed by immunofluorescence of the myoblast markers Desmin and MyoD, as well as expression of key markers as measured by qPCR (Figures 2A, S12, and S13A). Terminal differentiation of the myoblasts was performed over 3–6 days of culturing and confirmed by expression of the myogenic markers MyoD1, MyoG, and MYH3 using qPCR and immunofluorescence of the muscle markers MHC and MyoG (Figures 2A, S12, and S13A). Myogenic indices calculated after terminal differentiation (Figure S13B) at time points relevant for treatment were around 0.25, in line with other reported models.[16,25] Additionally, to maximize relevance of this model and treat cells at the most mature myogenic stage possible, we optimized treatment conditions such that PPMO gymnotic treatment was initiated 2 days after the terminal differentiation process had begun. Myogenic index was confirmed to be unaffected by compound treatment (Figure S13B).

Next, we characterized the splicing and expression of *GAA* in patient iPSC-derived myotubes. To evaluate the splicing of *GAA* in these models, we amplified the mis-spliced region of exons 1–5 by RT-PCR and submitted the PCR product for amplicon sequencing (Figure 2B). Canonical *GAA* splicing was found in the healthy control line, while several mis-spliced *GAA* variants were found in the patient-derived lines, in agreement with previous reports.[16] Furthermore, the individual expression of naturally occurring TV1 (NM_000152.5) TV2 (NM_001079803.3), and TV3 (NM_001079804.3) were analyzed by qPCR (Figure 2C). These findings demonstrated that TV2 was the most abundant transcript in all lines.

To determine if PPMOs are able to modulate *GAA* splicing in the disease-relevant model, we first used qPCR to measure expression of each *GAA* TV after a 3-day treatment with 20 μM RC-3002 (Figures 3A, 3B, and S13C). This analysis demonstrated that only TV1 and TV2 are affected by PPMO. Additionally, we confirmed the nature of the splicing correction and the absence of newly generated transcripts by amplicon sequencing (Figure 3C). This analysis additionally demonstrated correct restoration of the exon 1–2 junction upon PPMO treatment.

PPMO treatment corrects splicing in LOPD patient iPSC-derived myotubes

To determine the upstream effects of RC-3003 leading to increased GAA enzyme activity observed in patient fibroblasts, we treated differentiated patient iPSC-derived myotubes with RC-3003 delivered by gymnosis. First, we measured the amount of correct *GAA* splicing using a qPCR probe spanning the critical *GAA* exon 1–2 junction of TV1 and TV2 (Figure 4A). Treatment of patient iPSC myotubes with RC-3003 resulted in approximately a 4-fold increase in correctly spliced *GAA*, with a half maximal effective concentration of approximately 10 μM. Measuring total *GAA* transcript using a probe targeting all TVs confirmed an increase in *GAA* expression upon treatment (Figure 4B). Treatment of the same cell line with

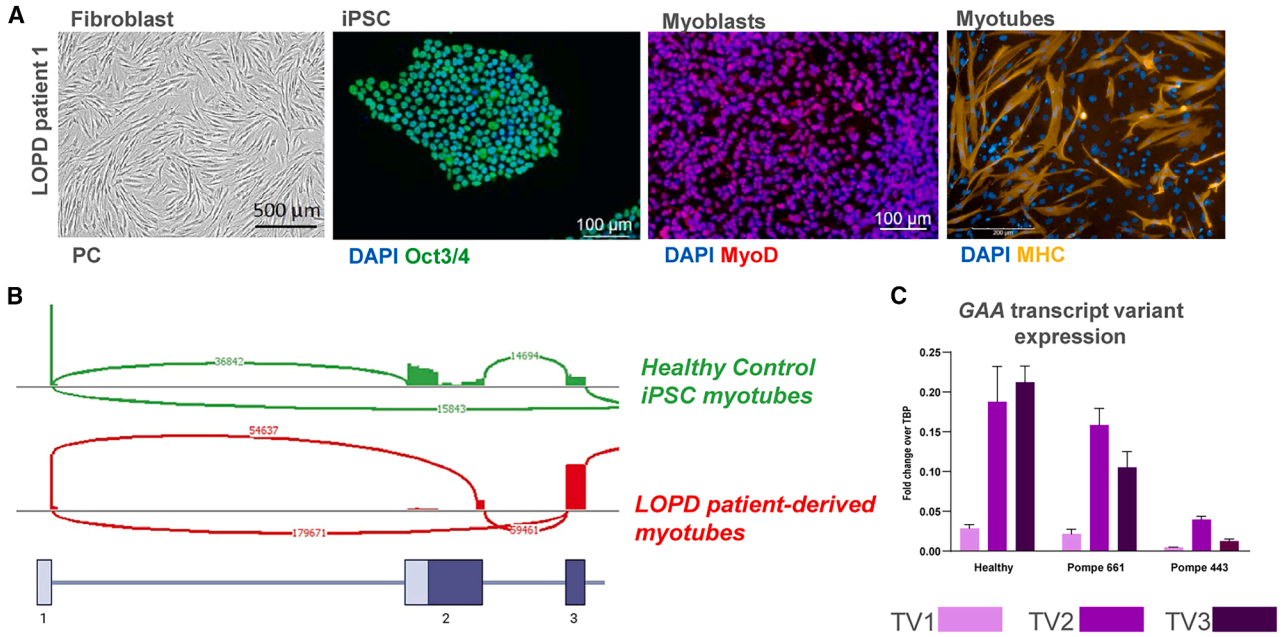

Figure 2. LOPD patient iPSC-derived myotubes recapitulate splicing deficits observed in LOPD patients

(A) LOPD patient fibroblasts were reprogrammed into iPSC lines and pluripotency was confirmed by immunostaining with OCT3/4. LOPD iPSCs were terminally differentiated into LOPD patient derived iPSC myoblasts and myotubes that express MYOD and MHC by immunostaining, respectively. PC, phase contrast. Scale bars: fibroblasts (500 µm), iPSC and myoblasts (100 µm), myotubes (200µm) (B) LOPD patient iPSC-derived myotubes faithfully recapitulate aberrant splicing reported in LOPD patients, including skipping of exon 2. C) *GAA* TV expression in LOPD patient iPSC-derived myotubes. TV1, NM_000152.5; TV2, NM_001079803.3; TV3, NM_001079804.3. Results are expressed as mean with error bars (SD).

20 µM RC-3003 led to a 2.1-fold increase in GAA protein in a dose-dependent fashion (Figures 4C and 4D). This increase was observed for both the primary translation product (110 kDa) as well as the post-translationally modified enzyme (70 kDa) (Figure 4C), which is trafficked to the lysosome.[26] Further downstream, a dose-dependent increase in lysosomal GAA enzyme activity was observed after gymnotic treatment with RC-3003 and led to approximately 2.6-fold increase in GAA enzyme activity after a single treatment (Figure 4E). Together these data support the proposed mechanism of PPMO-mediated correction of pathological IVS1 pre-mRNA splicing, followed by downstream increases upon treatment in both primary translation and post-translationally modified protein as well as lysosomal GAA enzyme activity.

Humanized LOPD mouse model recapitulates disease-causing splicing deficit

All of the reported murine models of PD involve the disruption of the endogenous mouse *Gaa* locus, and thus recapitulate many phenotypes of the less common infantile form of the disease.[27–29] To validate our precision genetic PPMO results, we sought to generate a murine model of the more prevalent[12,30] late-onset form of PD with the common IVS1 mutation. To accomplish this, we used CRISPR-CAS9 genomic engineering to insert the entire human IVS1-mutant genomic *GAA* sequence, including all 20 introns and exons (18 kb), into the murine *Rosa26* locus (Figures 5A and S14). The CAG promotor was used to drive widespread expression of IVS1-mutant human *GAA*. Genomes of founder mice were confirmed by PCR and Sanger sequencing, and germline transmission was established before characterization of third-generation mice (Figures S15 and S16). Animals were noted to be healthy and breeding normally. We used the *Rosa26* insertion strategy with the goal of single copy and stable genomic insertion.

To confirm and characterize the model at the molecular level, we first used genomic qPCR to confirm single copy insertion (Figure 5B) and used Sanger sequencing to confirm the predicted integration at the *Rosa26* locus (Figure S16). Next, *GAA* expression was confirmed in quadricep muscle by qPCR. As shown in Figure 5C, *GAA* TV2 was expressed to a higher degree compared with *GAA* TV1 and TV3, closely mirroring the *GAA* transcript expression pattern found in LOPD patient iPSC-derived myotubes (Figure 2C). We then assessed *GAA* expression in various tissues and found that the mutant human transgene, driven by the CAG promoter, was expressed at higher levels when compared with endogenous *Gaa* (Figure 5D). In quadriceps muscle, human *GAA* expression was 3- to 4-fold higher compared with *Gaa*.

Next, we sought to characterize the splicing of the human IVS1-mutant *GAA* transgene in LOPD mouse skeletal muscle, as it was unclear whether or how this mutation would disrupt splicing in the murine model. First, we extracted RNA from the quadriceps of LOPD animals and amplified the region between exons 1 and 5 by

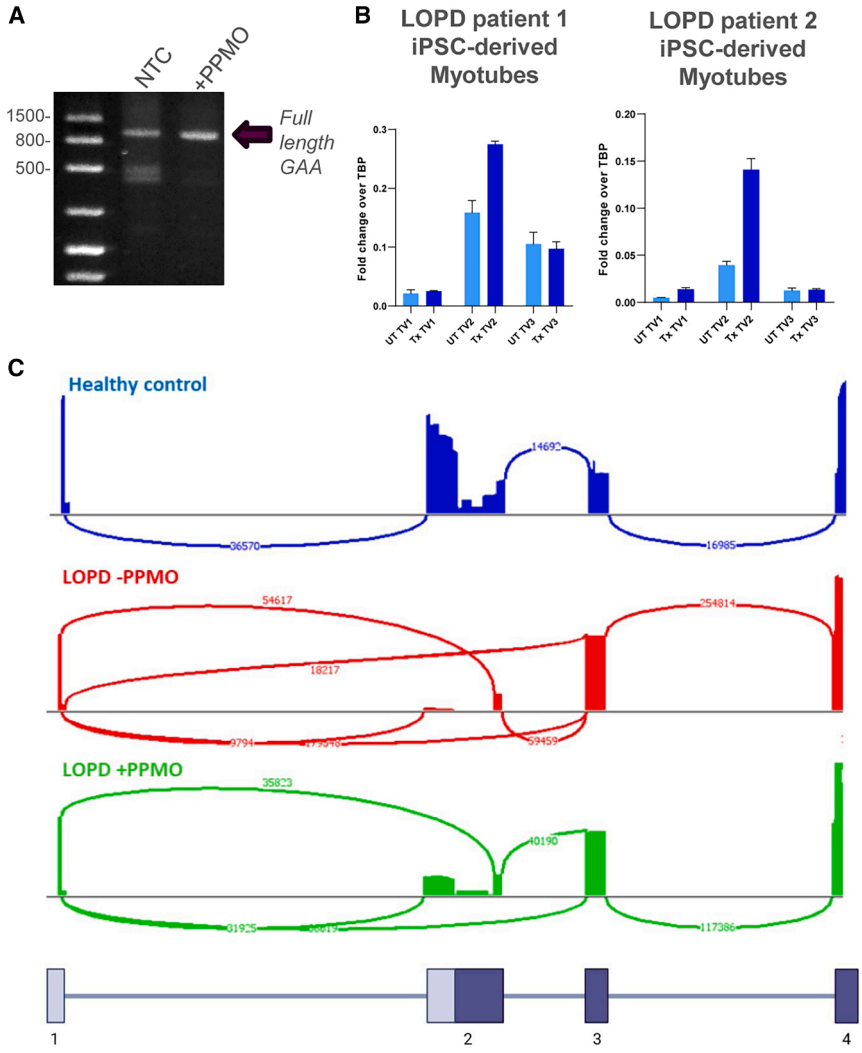

Figure 3. PPMO correct *GAA* splicing in LOPD patient iPSC-derived myotubes

(A) PPMO treatment decreases pathogenic splicing and increases full-length *GAA* as measured by endpoint RT-PCR. Marker in basepairs. Full-length *GAA*, 1100 bp; exon 2 skipping, 450 bp, 550 bp. (B) PPMO compounds increase levels of *GAA* TV1 and TV2 upon treatment. (C) PPMO treatment precisely restores the LOPD-critical *GAA* exon 1–2 junction with no detectable undesired splicing variants as measured by RNA amplicon sequencing. Results are expressed as mean with error bars (SD).

RT-PCR. Gel electrophoresis of the PCR products showed correctly spliced *GAA* along with several smaller, mis-spliced transcripts (Figure 5E) similar to the pattern found in patient iPSC myotubes (Figure 3B). The amplicon pool was subjected to amplicon sequencing, which confirmed that the human IVS1 *GAA* transgene mis-splicing in the LOPD mouse mirrored that observed in LOPD patients (Figure 5F). Accounting for TVs, we observed the same three major splice variants as found in LOPD patients.[16] These splice variants were additionally confirmed with unbiased standard RNA sequencing (Figure S17).

Next, we measured the relative amount of correctly and mis-spliced *GAA* in the LOPD mouse model. qPCR analysis measuring *GAA* splicing across the IVS1-defective exon 1–2 junction of TV1 and TV2 and total *GAA* at an unaffected exon junction indicated a similar relative ratio of correctly spliced to total *GAA* as compared with LOPD iPSC myotubes (approximately 0.4) (Figure S18).

Last, we sought to confirm that the expression of IVS1-mutant human *GAA* on murine *Gaa*$^{wt/wt}$ background did not elicit a muscle phenotype. To assess for morphological changes in muscle tissue, we analyzed quadricep and diaphragm muscle in 10-month-old mice by gross histology, which revealed no muscle-related abnormalities (Figure S19).

PPMO increases *GAA* expression and corrects pathological LOPD splicing *in vivo*

Having generated a suitable humanized model of LOPD that accurately reflects the pathological *GAA* splicing found in patients, we next sought to determine if PPMO are capable of correcting LOPD mis-splicing *in vivo*. As proof of concept, we injected LOPD mice with a single 100 mg/kg bolus IV dose of PPMO compound. After 7 days, animals were sacrificed and tissues collected for human *GAA* transcript analysis. In line with patient fibroblast and iPSC-derived myotube results, endpoint RT-PCR amplifying exons 1–5 of *GAA* in quadriceps muscle of mice treated with PPMO showed an increase in full-length *GAA* transcript compared with vehicle (Figure 6A). Amplicon sequencing of the PCR reaction pool demonstrated correction of *GAA* splicing (Figure 6B). The increase and splicing correction of *GAA* was quantified by qPCR, which indicated approximately 2-fold increase of *GAA* in quadricep and diaphragm tissues (Figure S20). These data support the target engagement and restoration of *GAA* transcript levels through correction of the pathogenic exon 1–2 mis-splicing.

To more fully quantitate and validate restoration, we treated animals with a single IV bolus dose of RC-3003 at either 30 mg/kg or 100 mg/kg. RNA was extracted from quadriceps tissue 7 days after injection and again subjected to PCR amplification of the region containing exon 1–5. Densitometric analysis indicated an increase from approximately 20% full-length *GAA* to approximately 50% full-length *GAA* (Figure S21A). qPCR analysis demonstrated a dose-dependent increase in *GAA* transcript, indicating approximately

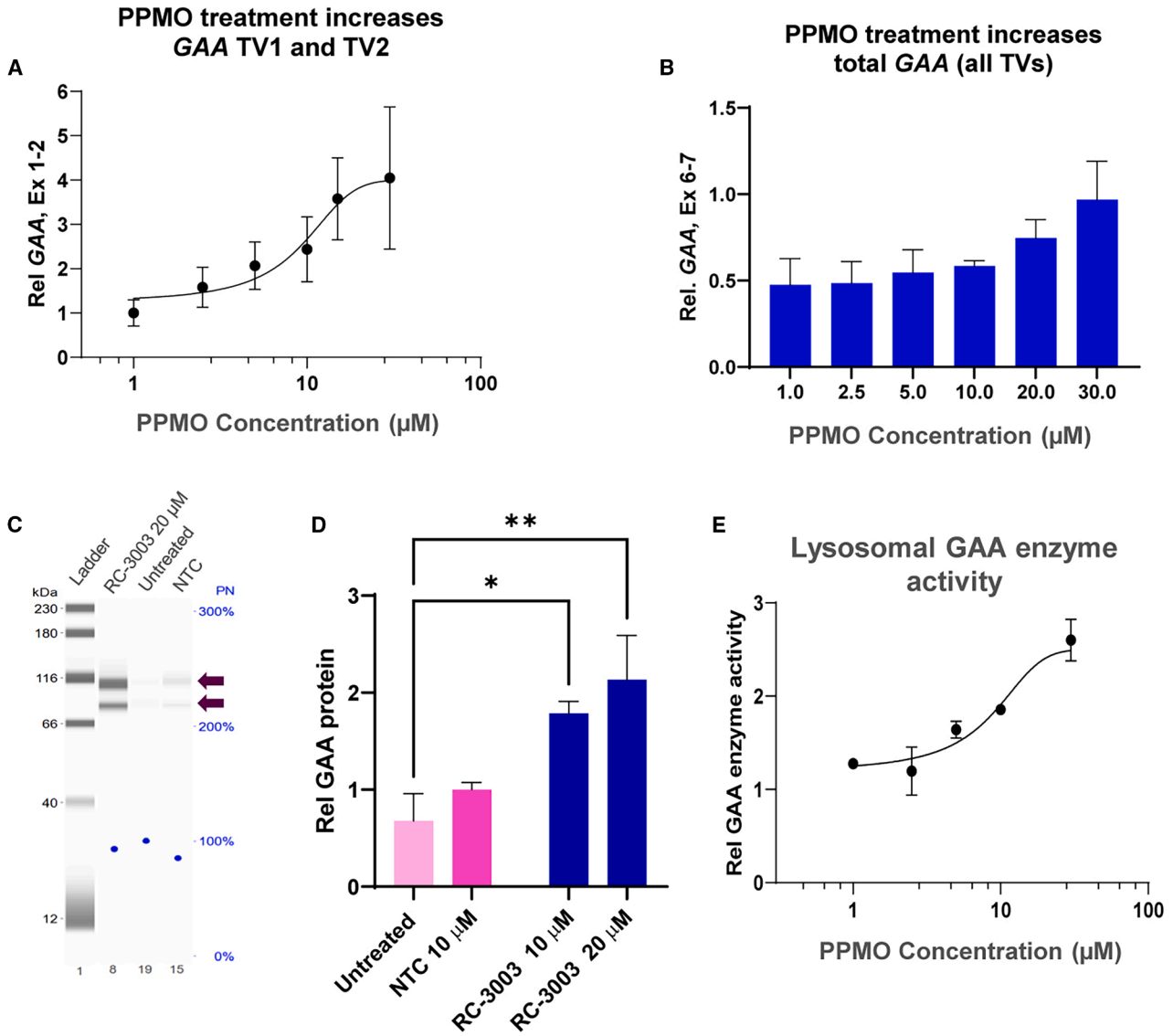

Figure 4. PPMO correct pathogenic *GAA* levels at transcript, protein, and lysosomal enzyme activity levels in LOPD patient iPSC-derived myotubes

(A) PPMO treatment increases *GAA* TV1 and TV2 at the LOPD critical exon 1-2 junction and also increases. (B) Total *GAA* (all TVs) transcript levels as measured by qPCR. (C and D) PPMO treatment similarly increases GAA protein (one-way ANOVA with Dunnett's multiple comparison test; $^{*}p < 0.05$; $^{**}p < 0.01$). Arrows indicate size of GAA primary translation (76 kDa) and post-translationally modified GAA (76 kDa). (E) Lysosomal GAA enzyme activity levels in patient iPSC-derived myotubes were increased after treatment with PPMO in a dose-dependent fashion. Results are expressed as mean with error bars (SD).

2-fold increase of *GAA* in skeletal muscle after the single dose of PPMO compound (Figure 6D). Additionally, the same analysis in liver and kidney tissues demonstrated lower efficacy in these off-target tissues (Figures S21B and S21C).

To understand high-level pharmacodynamics of RC-3003, we used an enzyme-linked oligonucleotide hybridization assay (ELOHA) to measure the amount of compound in quadricep tissues, which demonstrated a positive correlation between tissue compound concentration and compound efficacy (Figures 6D and S21D). Additionally, we assessed commonly used serum biomarkers of liver and kidney damage (blood urea nitrogen [BUN], creatinine [CRE], alanine transaminase [ALT], aspartate transaminase [AST]) 7 days after treatment, and found no elevations or other adverse safety signals or bodyweight changes (Figures 6E and S21E).

DISCUSSION

Standard of care for LOPD patients is currently limited to enzyme replacement therapies that are infused biweekly and come with limited efficacy and nearly unavoidable immune responses.

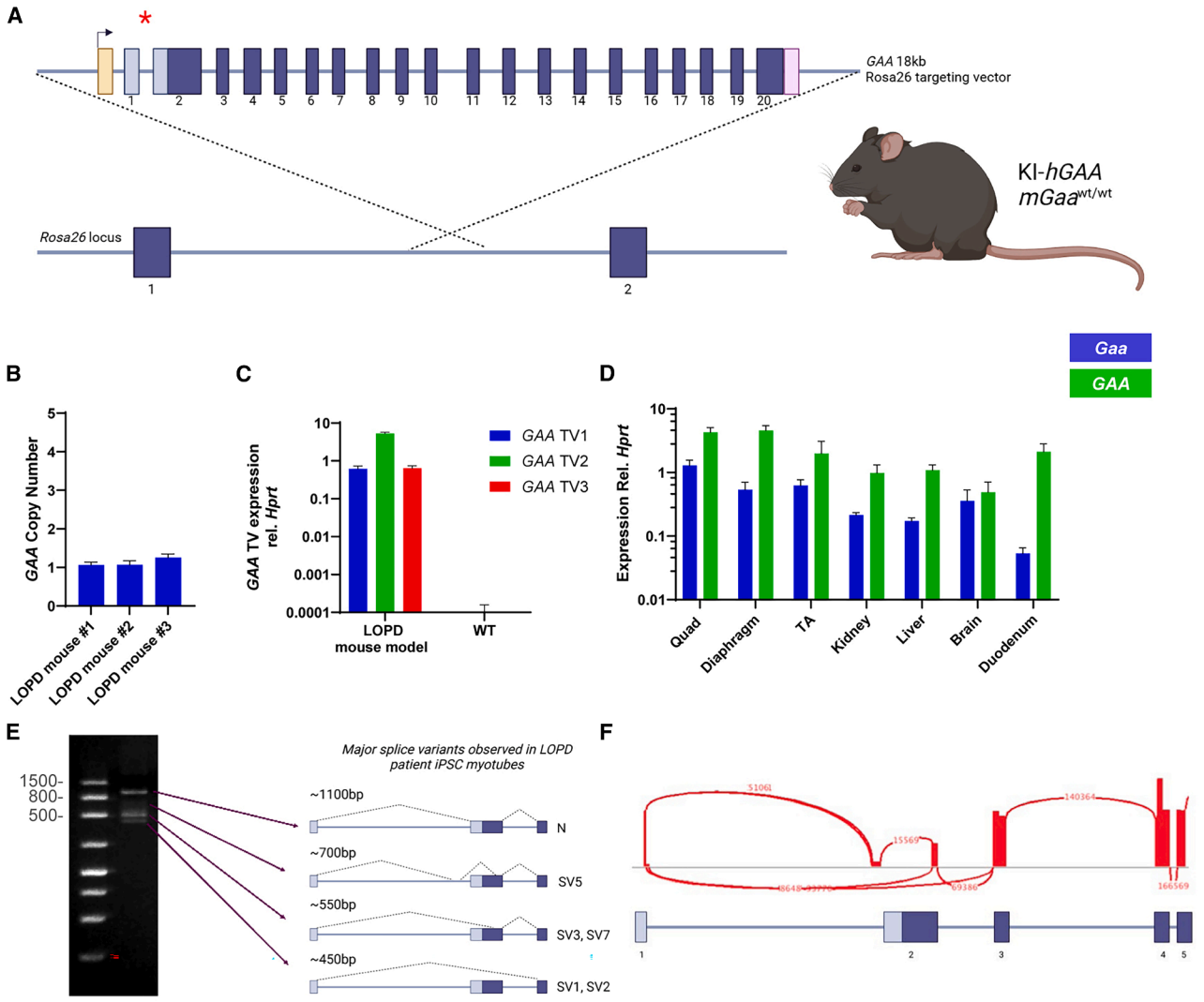

Figure 5. Generation and characterization of a relevant murine model of LOPD

(A) Human *GAA* harboring the IVS1 mutation was inserted into the *Rosa26* safe harbor locus. (B) Single copy integration was confirmed by genomic qPCR. (C) *GAA* TV expression in skeletal muscle was confirmed by qPCR. (D) *GAA* expression was confirmed in various tissues by qPCR analysis. (E) Endpoint RT-PCR analysis demonstrated that the mutant human *GAA* transgene was faithfully mis-spliced in the mouse and produced the same *GAA* splice variants found in LOPD patients. (F) *GAA* mis-splicing in mouse quadricep muscle was confirmed by RNA amplicon sequencing. Results are expressed as mean with error bars (SD).

However, these and earlier stage proposed treatments such as substrate reduction therapy targeting upstream glycogen synthesis, do not target the genetic basis of LOPD. Recent newborn screening results indicate the IVS1 mutation is more prevalent in the United States than previously estimated, upwards of 1:30,000.[12,14] Given the widely recognized unmet need for these patients, a precision genetic medicines approach for these patients would come closer to addressing the fundamental defect.

Here we demonstrate the efficacy of RC-3003, a PPMO compound that is active in skeletal muscle, targets the IVS1 mutation, and corrects the pathological splicing found in IVS1-mutant LOPD patients. First, we screened PPMO compounds *in vitro* that led to the identification of RC-3001, which increased GAA enzyme activity levels approximately 2- to 3-fold in patient fibroblasts after a single treatment but demonstrated cytotoxicity *in vitro*. We mitigated *in vitro* cytotoxicity by optimizing the sequence with an abasic subunit resulting in the identification of RC-3003. The efficacy of this compound was measured in two patient fibroblast lines versus healthy with similar results.

Since LOPD symptoms primarily manifest in skeletal muscle, we additionally validated the efficacy of RC-3003 in patient iPSC-derived myotubes. Here we showed that PPMO compounds correct

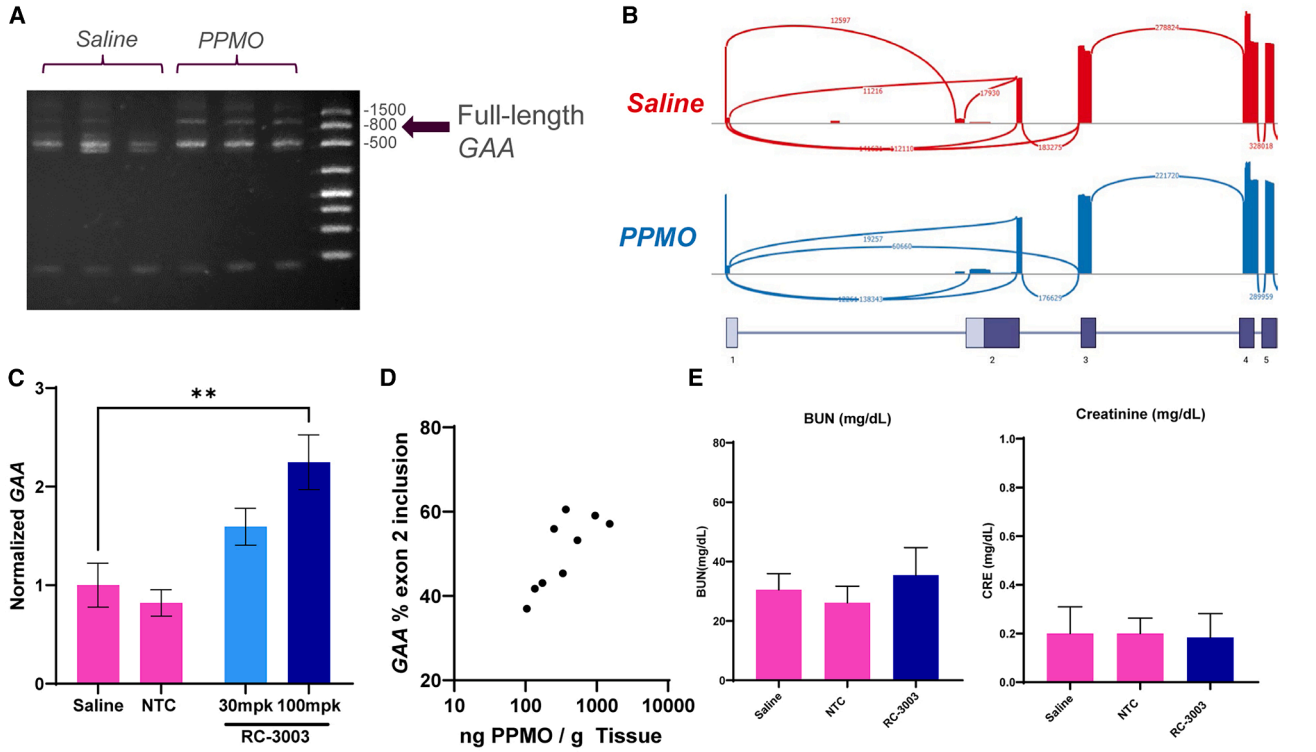

Figure 6. Systemic PPMO treatment corrects *GAA* splicing *in vivo*

(A) Endpoint RT-PCR qualitatively showed an increase in full-length *GAA* after single IV dose of RC-3002. (B) Amplicon sequencing confirmed an increase in correctly spliced exon 1–2 junction upon treatment with RC-3002. (C) qPCR analysis of RNA extracted from quadricep muscle of animals treated with a single dose of RC-3003 demonstrated a dose-dependent increase in *GAA* transcript levels that was found to correlate with (D) compound tissue concentrations. (E) treatment was well tolerated. One-way ANOVA with Dunnett's multiple comparison test. $^{**}p < 0.01$. Results are expressed as mean with error bars (SD).

the pathogenic IVS1 splicing found in LOPD patient muscle cells, and that this correction leads to an increase in downstream GAA protein levels. We note that GAA is post-translationally modified and transported to the lysosome where it is modified to its functional form. We observed an increase in both the primary translation and post translationally modified forms of GAA protein. Additionally, in agreement with results obtained in patient fibroblasts, we documented increased GAA enzyme activity levels in patient iPSC myotube cellular lysates after a single 4-day treatment with RC-3003. These results help us to understand the mechanism of action of PPMO compounds targeting the faulty IVS1 mutation.

Previous *in vitro* work noted a disconnect between *GAA* splicing and GAA enzyme activity correction.[16] We show that PPMO compounds here modulate specific TVs, and taking this into consideration measured consistent results between the total of *GAA* transcript levels, protein, and lysosomal enzyme activity.

Since no animal models of LOPD existed, we generated a mouse model of LOPD with the IVS1 mutation to assess target engagement of optimized PPMO *in vivo*. Precision genetic medicines such as PPMO compounds affect mRNA splicing, thus necessitating the insertion of the entire human genomic *GAA* sequence (approximately 18 kb). We used CRISPR-CAS9 engineering to insert the entire genomic sequence including the IVS1 mutation into the *Rosa26* safe harbor locus. Central to the successful generation of this model was recapitulation of the many mis-splicing events found in LOPD patients.[17] Gratifyingly, we found this model did recapitulate all of the reported LOPD splice variants, and thus could serve as a good model to assess precision genetic medicines tailored to the IVS1 mutation. Considering the primary purpose of this model was to evaluate target engagement, we opted to use the CAG promoter to drive high and widespread expression of the LOPD transgene and note the overall expression levels are significantly higher than endogenous mouse *Gaa*.

Indeed, 7 days after a single IV dose of PPMO compound, successful target engagement was measured at the transcript level. qPCR analysis of human *GAA* in the $GAA^{LOPD-IVS1/-}$ model indicated approximately 2- to 3-fold increase of human *GAA* upon treatment. We further visualized all splice junctions of the first 5 *GAA* exons to confirm no aberrant or new splice variants were produced after treatment. This analysis additionally indicated the restoration of the critical exon 1–2 junction. We validated this restoration by demonstrating that splicing restoration was dose-dependent and positively correlated to tissue compound concentration.

Additionally, we showed PPMO compounds are well tolerated and had limited activity in off-target organs such as liver and kidney.

Due to the wide spectrum of GAA enzyme activity levels found in healthy individuals, it is unclear what levels are needed to abolish or delay LOPD symptom onset. We note that pseudodeficient carriers of IOPD are unaffected, and that recent newborn screening efforts have set a threshold of 18% GAA enzyme activity assay in initial screens.[15] Additionally, recent data using cultured patient fibroblasts suggest that doubling GAA enzyme activity would increase levels in LOPD patients above the disease threshold.[31]

Additionally, recent work has established a genetic modifier to LOPD splicing that results in a more aggressive phenotype and earlier symptom onset.[32] We note the higher proportion of splice variant 2 in these patients and the demonstrated efficacy here of PPMO compounds to correct this variant *in vitro* and *in vivo*.

Together, the data outlined here demonstrate the mechanism of action and successful GAA restoration in LOPD patient iPSC myotubes, coupled with the ability to penetrate muscle tissue and similarly correct pathogenic *GAA* splicing *in vivo*.

MATERIALS AND METHODS

Synthesis of PMO

The general procedure for synthesis of PMO is described in the supplemental information (materials and methods, Tables S2 and S3; Figures S22 and S23).

General procedure for the synthesis of PPMO

All the PPMOs used in this study were synthesized in a similar fashion as described in this section. We have described the synthesis of **RC-3003 PPMO** in detail, as an example.

In a dry vial, **RC-3003 PMO** (4 g, 0.5 mmol) was dissolved in 40 mL of DMSO. In a separate vial, the peptide Ac-R_6G-COOH (794 mg, 0.753 mmol) was dissolved in 30 mL of DMSO and activated using HATU (382 mg, 1 mmol). Next, the activated peptide solution was added to vial containing solution of **RC-3003 PMO** and DIPEA (195 mg, 262 μL, 1.51 mmol) was added to it, and the reaction mixture was stirred at 35°C for 2 h. The progress of the reaction was monitored by LC/MS until **RC-3003 PMO** was fully consumed. The reaction mixture was then purified by preparative cation exchange chromatography on a NanoSP-15L column (150 × 10 mm, 15 μM) with solvent A (20 mM sodium phosphate buffer +20% CH_3CN) and solvent B (solvent A + 0.8 M NaCl) using a gradient of 0%–60% solvent B over 120 min at RT. The pure fractions were collected and desalted using the same procedure as mentioned above and lyophilized to produce the final product RC-3003 PMO (2.53 g, 0.28 mmol, 56%) as a white fluffy solid.

Characterization of PPMOs

All the PPMOs used in this study were characterized by strong cation exchange chromatography (SCX), SEC, and liquid chromatography (LC) electrospray ionization mass spectrometry. A stock solution of the PPMOs (0.5 mg/mL) was prepared in nuclease free water and 5–10 μL of the solution was injected on the SCX-high-performance LC (HPLC), SEC-HPLC, and LC mass spectrometry for analysis.

For SCX-HPLC, the compounds were analyzed on an SCX-20 column (Thermo Fisher Scientific; 4 × 250 mm, 10 μm) under native SCX-HPLC (solvent A: 24 mM H_3PO_4, 25% CH_3CN, pH = 2; solvent B: solvent A + 1 M KCl, pH = 2) using a gradient of 0%–95% solvent B over 13 min at 40°C. For PPMOs exhibiting secondary structures (or homodimer formation) under native SCX conditions, a denaturing condition was employed to further analyze them. For the denaturing SCX-HPLC, compounds were analyzed on the same column, using the same temperature and gradient but with solvent A (0.1% TFA, 20% CH_3CN) and solvent B (solvent A + 1.5 M Gn.HCl).

For SEC-HPLC, compounds were analyzed on a Zenix SEC-150 column (Sepax; 7.8 × 300 mm, 3 μm) with 0.1 M sodium phosphate buffer (pH = 7.3) using an isocratic gradient over 20 min.

For ESI-MS, the compounds were analyzed on a 1260 Infinity II LC (Agilent) using a Poroshell 120 EC-C18 column (Agilent; 3 × 50 mm, 2.7 μm) followed by mass detection on a 6230 TOF-MS (Agilent) under positive ESI mode. A representative PPMO structure is shown in Figure S24.

Generation of an LOPD mouse model

All animal studies were conducted with the approval of the Institutional Animal Care and Use Committee at Sarepta and performed according to their guidelines. The LOPD knockin mouse model was generated by inserting human *GAA* gene into the *Rosa26* locus of C57BL/6 mice using CRISPR-Cas9 genome engineering (Cyagen Biosciences). First, a BAC clone containing human *GAA* was selected and the IVS1 mutation introduced by a positive/negative homologous recombination selection scheme. The modified gene was subcloned to introduce the CAG promoter and PolyA tail. The entire CAG-(IVS1)h*GAA*-polyA insert was sequenced and cloned into intron 1 of the *Rosa26* locus in reverse orientation. *Rosa26* homology arms were amplified by PCR and the resulting targeting vector along with Cas9 and gRNA were co-injected into fertilized eggs.

Founder knockin mice were genotyped first for the presence of human *GAA* in the *Rosa26* locus, then for the presence of targeting vector to assess for potential random integration. Mice determined to contain human *GAA*, but no targeting vector were confirmed to harbor the *GAA* IVS1 mutation and correct *Rosa26* insertion by Sanger sequencing, then bred further to establish germline transmission. One F0 founder line was confirmed with germline transmission of the human *GAA* insert in the *Rosa26* locus.

LOPD mouse model genomic copy number analysis

We mechanically homogenized 10–20 mg of fresh LOPD murine tail or ear tissue with a metal bead beater using the *Quick*-DNA 96 kit (Zymo Research) lysis buffer. Total DNA was isolated following

the kit protocol and diluted 5–10× before use. We amplified 1 μL of DNA in a PCR reaction containing an assay for human GAA detection on the VIC channel (Hs03961696_cn, Thermo Fisher Scientific) and mouse Tfrc (Thermo Fisher Scientific) on the VIC channel using Genotyping Master Mix (Thermo Fisher Scientific, Quantstudio 7 Pro). A relative standard curve for the duplex qPCR reaction was generated using a 1:1 mixture of mouse gDNA (Promega) and human gDNA (Promega). The relative quantity of human GAA was calculated for each sample and normalized to Tfrc.

Histological analysis of LOPD KI mouse

Ten 10-month-old LOPD knockin and three age-matched wildtype control mice were sacrificed. Both quadriceps and diaphragm muscles were excised and immersion-fixed in 4% paraformaldehyde for 24 h then transferred to 70% EtOH. The fixed left and right quadriceps muscle and the diaphragm muscles were submitted to Premier Labs, LLC where they were processed, sectioned, and stained with hematoxylin and eosin (H&E). For each sample, a single H&E slide along with a serial periodic acid–Schiff stained slide was made. All glass slides were submitted to Charter Preclinical Services for imaging.

LOPD mouse model gene expression analysis

We mechanically homogenized 10–20 mg of snap frozen LOPD murine tissue with a metal bead beater and RNA extracted using the Chemagic 360 RNA system (PerkinElmer). RNA (0.5–1.0 μg) was reverse transcribed using the superscript VILO kit (Thermo Fisher Scientific) according to the manufacturers protocol. A multiplex qPCR assay measuring GAA expression (Hs.PT.58.4293297.gs, IDT) on the FAM channel, and GAPDH (Mm99999915_g1, Thermo Fisher Scientific) on the VIC channel was used with Multiplex Master Mix (Thermo Fisher Scientific) on a Quantstudio 7 Pro PCR thermocycler (Thermo Fisher Scientific).

ELOHA

For the ELOHA, oligonucleotide capture probes with a 5AmC12 modification were designed to hybridize to the 5′ end of the PPMO sequence. These capture probes were covalently attached to Pierce Maleic Anhydride Activated Plates (CN: 15110, Thermo Fisher Scientific) by incubating coating solution (500 nM capture probe, 2.5% sodium bicarbonate solution) for 1 h at 37°C. Plates were then washed and blocked overnight with 10% milk/PBST at 4°C. Tissue samples were lysed in 20 μL of ELOHA lysis buffer (10 mM Tris-HCl pH 7.5, 0.5% IGEPAL, 100 mM NaCl, 5 mM EDTA) per milligram of protein before being digested with Proteinase K (Qiagen cat# 19133) at a final concentration of 1 mg/mL for 60°C for 30 min. We then incubated 30 μL of this digested lysate with 120 μL Detection Probe Solution (333 nM biotinylated [3BioTEG modified] oligonucleotide detection probe targeting the 3′ sequence of the PPMO, 500 mM guanidine thiocyanate, 0.04% lauryl sarcosine, 3 mM sodium citrate, and 1.25 mM DTT in PBST). These samples were then incubated overnight at 4°C in the blocked, capture probe coated maleic anhydride plate. The next day, plates were washed 3× with PBST before incubation with streptavidin-AP-conjugate (CN: 11093266910, Sigma-Aldrich) for 1 h. Plates were washed 3× more with PBST and AttoPhos AP Fluorescent Substrate System (CN: S1000; Promega) was added for 20 min before the reaction was stopped with 10 μL of EDTA (0.5 M solution/pH 8.0) (CN: BP2482100; Thermo Fisher Scientific). Fluorescence was read using a Spectramax i3 reader to determine tissue compound concentrations (Ex 440, Em 555).

LOPD mouse model percent splicing correction analysis

We mechanically homogenized 10–20 mg of snap frozen LOPD murine tissue with a metal bead beater and RNA extracted using the Chemagic 360 RNA system (PerkinElmer). RNA (0.5–1.0 μg) was reverse transcribed using the Maxima H Minus cDNA Synthesis Master Mix (CN: M1662; Thermo Fisher Scientific) according to the manufacturers protocol. PCR reaction with primer F: GGAAA CTGAGGCACGGAGCG (exon 1) and primer R: GGACCACATC CATGGCATTGC (exon 5–6) were used to amplify *GAA*. Thermal cycle programmed for 5 min at 95°C for initial denaturation, followed by 44 cycles of 30 s at 95°C for denaturing, 30 s at 60°C for annealing, 2 min at 72°C for extension, and a final extension at 72°C for 2 min. PCR Products were analyzed using a LabChip GX Touch Nucleic Acid Analyzer (Revvity), the DNA 1K/12K/Hi Sensitivity Assay LabChip (PN 760517; Revvity), and DNA 1K Reagent Kit LabChip DNA assay (PN: CLS760673; Revvity) according to the manufacturers protocol. The software Bio-Rad CFX Maestro was used to quantify bands for correctly spliced (1,050 bp) and splice variants (750 bp, 550 bp, 450 bp). Percent correctly spliced was determined by dividing the amount of 1,050 bp by the sum of all bands.

LDH cytotoxicity assay in eGFP HeLa cells

HeLa cells expressing eGFP (IVS2-654)[33] were expanded in HeLa media (DMEM [CN:10566016, Gibco] supplemented with 5% horse serum [CN: 16050122, Gibco], 5% fetal bovine serum [FBS] [CN: SH30071.03, Cytiva], 200 μg/mL Geneticin [CN: 11811-031, Gibco], 2 mM L-glut [CN: 25030-149, Gibco]) and seeded at 25,000 cells/well in 96-well plates (CN: 353072; Corning). At 24 h after seeding, media was changed to 100 μL of HeLa media containing indicated concentrations of PPMO. A CytoTox 96 Non-Radioactive Cytotoxicity Assay (CN: G1780; Promega) kit was used after 18 h of exposure to measure LDH. We transferred 50 μL of media per well to a fresh 96-well plate, and 50 μL of the CytoTox 96 Reagent was added to each sample aliquot. The plate was covered with foil to protect it from light and incubated for 30 min at room temperature. We added 50 μL of stop solution after the incubation, and absorbance was read at 490 nm using a Spectramax i3 reader. A maximum LDH release control was generated by adding 10 μL of 10X Lysis Solution (provided by the kit) to positive control wells 45 min before performing the assay. Percent cytotoxicity = 100 × (experimental LDH Release (OD_{490})/maximum LDH Release(OD_{490})).

Serum analysis

Upon study takedown, whole blood was collected and centrifuged at 2,000 rcf for 10 min at 4°C. We froze 70 μL of serum at −80°C and

transferred for analysis to IDEXX Bioanalytics for analysis of BUN, CRE, ALT, and AST.

LOPD patient iPSC-derived myotubes gene expression analysis

Patient iPSC-derived myoblasts were seeded in a 96-well or 24-well collagen-coated plate (Corning) and expanded in iPSC-derived myoblast expansion medium (iXCells Biotechnologies) for 48 h. Media was changed to myotube differentiation media (iXCells Biotechnologies) and differentiation was continued for 48 h. Media was then changed to fresh differentiation media containing the indicated concentrations of PPMO. RNA was extracted from cell cultures after 72 h of gymnotic treatment using the *Quick*-RNA 96 Kit (Zymo) following the manufacture's protocol. We reverse transcribed 100–300 ng of RNA using the superscript VILO kit (Thermo Fisher Scientific) according to the manufacturers protocol. A multiplex qPCR assay measuring *GAA* expression at the exon 1–2 locus (Hs.PT.58.24962380, Integrated DNA Technologies, 900 nM primers, 250 nM probe) on the FAM channel, *GAA* at the exon 3–4 locus (Hs01089834_m1, Thermo Fisher Scientific, 1.8 μM primers, 500 nM probe) on the VIC channel, and HPRT (Hs999 99909_m1_qsy, Thermo Fisher Scientific, 900 nM primers, 250 nM probe) on the JUN channel was used with Multiplex Master Mix (Thermo Fisher Scientific) on a Quantstudio 7 Pro PCR thermocycler (Thermo Fisher Scientific). qPCR cycling conditions consisted of an initial denaturation step for 20 s at 95°C, followed by 40 cycles of 95°C for 3 s, 58°C for 20 s with a 1.92°C per second ramp rate.

Western blot analysis

Cell lysates were prepared using RIPA lysis buffer (Thermo Fisher Scientific). Protein concentration was measured using Pierce BCA Assay Kit (Thermo Fisher Scientific). Cell lysates were prepared using the sample preparation kit (Proteinsimple) for an automated capillary western blot system, JESS system (Proteinsimple). Cell lysates were diluted to the same protein concentrations using the 0.1× sample buffer (Proteinsimple) and mixed with 5× fluorescence master mix (Proteinsimple) according to protocol instructions. Samples were denatured at 95°C following protocol instructions. JESS was run using a 1:400 diluted anti-GAA primary antibody (Abcam ab137068) diluted with milk-free antibody diluent; protein normalization substrate; horseradish peroxidase-conjugated secondary antibodies; chemiluminescence substrate; and wash buffer dispensed into indicated wells of the assay plate. Samples were loaded in the indicated locations on the JESS plate in triplicate with the biotinylated ladder marker and the assay plate was placed in the JESS apparatus. Signal intensity (peak area) of the protein was normalized to the peak area of the total protein included in the capillary well using the protein normalization kit and analysis on Compass Software (Proteinsimple). Quantitative analysis of GAA protein bands was performed using the Compass Software (ProteinSimple).

GAA enzyme activity for LOPD patient fibroblasts

Fibroblasts were plated in 24-well cell culture plates at 30,000 cells/well and incubated overnight. Cells were then washed in PBS and then treated with PPMO-supplemented media via gymosis. Cells were allowed to incubate with treatment and no media changes for 6 days. For GAA Activity Assay lysis, cells were washed once with PBS and then lysed (freeze/thaw 10 min, −80°C) in ice-cold GAA Activity Assay Buffer (Abcam). Cell lysates were centrifuged, and the supernatants were used in triplicate for GAA Enzyme Activity Assay. Protein concentration was measured using Pierce BCA Assay kit (Thermo Fisher Scientific). The GAA Enzyme Activity Assay was run following the kit instructions. The resulting fluorescence was read on the SpectraMax i3 spectrometer (Molecular Devices) at excitation 485 nm and emission 535 nm.

GAA enzyme activity assay for LOPD patient iPSC-derived myotubes

Patient iPSC-derived myoblasts were plated in 24-well collagen-coated plates (Thermo Fisher Scientific) at 80,000 cells/well in Expansion Media (EM, iXCells Biotechnologies). After 48 h of growth in EM, cells were washed in PBS and media is changed to Differentiation Media (DM, iXCells Biotechnologies). Cells were incubated in DM for 48 h, then treated with PPMO-supplemented DM and incubated without media changes for 4 days. For GAA Activity Assay, cells were lifted, pelleted, then lysed in ice-cold GAA Activity Assay Buffer (Abcam). Protein concentration was measured using Pierce BCA Assay kit (Thermo Fisher Scientific). The GAA Enzyme Activity Assay was run following the kit instructions. The resulting fluorescence was read on the SpectraMax i3 spectrometer (Molecular Devices) at excitation 485 nm and emission 535 nm.

GAA TV expression analysis

cDNA from LOPD mouse quadricep muscle or LOPD patient iPSC-derived myotubes was amplified using PowerUp SYBR Green Master mix (Thermo Fisher Scientific) on a Bio-Rad PCR thermocycler (Bio-Rad) using GAA TV1, TV2, or TV3 primers according to the manufacturer protocol. Relative quantities of each TV were normalized to mouse Hprt (Mm.PT.39a.22214828, Integrated DNA Technologies).

Endpoint PCR

cDNA from LOPD mouse quadricep muscle was amplified in a PCR reaction. *GAA* exons 1–5 were amplified using primers GAA Ex1–5 Fwd and GAA Ex1–5 Rev (Table S4) with LA Taq Polymerase with GC Buffer (TaKaRa) following the manufacturer's protocol using a Bio-Rad PCR thermocycler. PCR amplification products were visualized using a 2.2% agarose gel (Flashgel System, Lonza).

Splice variant analysis

Endpoint PCR reactions using LOPD mouse quadricep cDNA were purified using the QIAquick PCR Purification Kit (Qiagen). The mixture was subjected to Amplicon-EZ MiSeq 2 × 150 bp sequencing (Azenta) resulting in more than 200,000 unfragmented reads per sample (>75 bp). The reads were aligned to *GAA* on the human reference genome (GRCh38) using the STAR (Spliced Transcripts Alignment to a Reference) aligner.

Junctions with greater than 5,000 exon-spanning reads were visualized using Integrated Genomics Viewer (Broad Institute). Total RNA-seq was carried out from snap frozen LOPD mouse quadricep tissue (Azenta). More than 100M total reads obtained were similarly mapped and visualized.

Fibroblast cell cultures

Human fibroblast cell lines were maintained in modified eagle medium (MEM, Thermo Fisher Scientific) containing 15% FBS and 2 mM L-glutamine at 37°C incubator with 5% CO_2. Fibroblast cell lines currently used were obtained from Coriell Institute and include the following lines: GM08402 (healthy control), GM08400 (healthy control), GM00443 (Pompe late-onset), GM11661 (Pompe late-onset), GM20089 (Pompe infantile onset), and GM20123 (healthy Pompe carrier). One day before treatment cells were plated in 24-well cell culture plates at 30,000 cells/well and incubated overnight. Cells were then washed in PBS and a treatment of PPMO supplemented with media was added to wells. Cells were allowed to incubate with treatment and no media changes for 6 days.

Non-integrative reprogramming of LOPD patient fibroblasts into iPSC

The fibroblasts were maintained in DMEM 10% FCS. After overnight incubation, culture medium was replaced with a fresh one, and cells were transfected with 2 μg of episomal plasmids from Epi5 iPSC Reprogramming Kit (Themo Fisher Scientific) by using FuGENE6 transfection reagent (Promega). The next day, culture medium was replaced with mTeSR-plus medium (StemCell Technologies). During the reprogramming process, transfected cells were cultured in mTeSR plus, and the medium was changed every other day up to 2 weeks post transfection. Colonies were transferred onto new culture dishes covered with Geltrex matrix by using a pipette tip. An hour before the procedure, 10 μM Y-27632 was added to the culture medium. The iPSCs were further propagated and maintained in mTeSR plus medium as described previously.[34]

Patient iPSC-derived myoblast SKM differentiation

Myogenic progenitors were differentiated from hiPSCs according to the protocols described previously.[35] Briefly, myogenic progenitors were generated through a multi-step small molecule differentiation protocol. Myogenic progenitors were expanded, passaged, and cryopreserved in 60 μg/mL collagen I-coated six-well plates. For myoblast differentiation, frozen myogenic progenitors were thawed in myoblast expansion medium (iXCells, Cat. # MD-0102A). Growth medium was refreshed every 2 days for 8 days then cryopreserved. For myotube differentiation, the myoblasts were recovered and seeded at a density of 32,000/cm^2 and cultured using myoblast expansion medium to reach 100% confluency. For skeletal muscle cell differentiation, confluent myoblast cultures were switched over to myoblast differentiation medium (iXCells, Cat.# MD-0102B) with media changes every 2 days. Elongated myotubes were evident after 72 h in myoblast differentiation medium.

LOPD patient fibroblast lines GM00443 and GM11661 were obtained (Coriell) and reprogrammed to iPSC lines via a feeder-free and footprint-free method (iXCells Biotechnologies). Pluripotency of iPSC lines was verified by immunostaining for MHC and MyoG.

Statistics

Statistical analysis was conducted using a one-way ANOVA test with Dunnett's multiple comparison test. Results were presented as mean ± standard deviation (SD), with a p value of less than 0.05 was considered to indicate statistical significance. Stars designate statistical significance (****$p < 0.0001$, ***$p < 0.005$, **$p < 0.01$, *$p < 0.05$).

For a comparison between more than two groups, ANOVA followed by the Holm-Sidak post hoc test was used to determine the statistical significance among groups. Two-sided p values of less than 0.05 were considered to indicate statistical significance.

DATA AVAILABILITY

All data are available in the main text or the supplementary materials. All data supporting the findings of this study are available from the corresponding author upon reasonable request.

ACKNOWLEDGMENTS

Funding was provided by Sarepta Therapeutics, Inc. Graphical figures were generated with BioRender.

AUTHOR CONTRIBUTIONS

R.A.O., K.J.K., and A.B.M. were responsible for conceptualization and methodology of the study. M.E.A., P.G.C., T.J., A.B., K.Y.M., K.H., K.A., N.J., N.L., A.M., C.D.G., A.M.W., E.G.T., S.G., E.C., S.A., X.T., A.J.C., and B.Z.C. were responsible for investigations and sample processing. R.A.O., K.J.K., and A.B.M. were responsible for supervision. R.A.O. and A.B.M. were responsible for writing the original draft. R.A.O., K.J.K., A.B.M., and K.Y.M. were responsible for draft review and editing.

DECLARATION OF INTERESTS

All authors were employees of Sarepta Therapeutics during the course of this work. R.A.O. is currently an employee of Aliada Therapeutics. M.E.A. is currently an employee of Jnana Therapeutics. T.J. is currently an employee of Editas Medicines. X.T. is currently an employee of Intellia Therapeutics. A.J.C. is currently an employee of Amgen. K.J.K. is currently an employee of MiRecule. A.B.M. is currently an employee of Foresite Labs.

Two patents cover this work: Pompe Disease Mouse Model Generation, Characterization and Methods of Use Pompe Disease Mouse Model Generation, Characterization and Methods of Use US patent application 63/377,516 WO/2024/073404 · September 26, 2023.

Antisense Oligonucleotides Having One or More Abasic Subunits Antisense Oligonucleotides Having One or More Abasic Subunits US patent application US2022/044995 WO/2023/055774A1 · September 28, 2022.

SUPPLEMENTAL INFORMATION

Supplemental information can be found online at https://doi.org/10.1016/j.omtn.2025.102524.

REFERENCES

1. Vanherpe, P., Fieuws, S., D'Hondt, A., Bleyenheuft, C., Demaerel, P., De Bleecker, J., Van den Bergh, P., Baets, J., Remiche, G., Verhoeven, K., et al. (2020). Late-onset Pompe disease (LOPD) in Belgium: clinical characteristics and outcome measures. Orphanet J. Rare Dis. *15*, 83.

2. Hagemans, M.L.C., Winkel, L.P.F., Van Doorn, P.A., Hop, W.J.C., Loonen, M.C.B., Reuser, A.J.J., and Van der Ploeg, A.T. (2005). Clinical manifestation and natural course of late-onset Pompe's disease in 54 Dutch patients. Brain *128*, 671–677.
3. Toscano, A., Rodolico, C., and Musumeci, O. (2019). Multisystem late onset Pompe disease (LOPD): an update on clinical aspects. Ann. Transl. Med. *7*, 284.
4. Sarah, B., Giovanna, B., Emanuela, K., Nadi, N., Josè, V., and Alberto, P. (2022). Clinical efficacy of the enzyme replacement therapy in patients with late-onset Pompe disease: a systematic review and a meta-analysis. J. Neurol. *269*, 733–741.
5. Raben, N., Roberts, A., and Plotz, P.H. (2007). Role of autophagy in the pathogenesis of Pompe disease. Acta Myol. *26*, 45–48.
6. Guemy, C., and Laforet, P. (2023). The new horizons for treatment of Late-Onset Pompe Disease (LOPD). Rev. Neurol. (Paris) *179*, 81–89.
7. Wencel, M., Shaibani, A., Goyal, N.A., Dimachkie, M.M., Trivedi, J., Johnson, N.E., Gutmann, L., Wicklund, M.P., Bandyopadhay, S., Genge, A.L., et al. (2021). Investigating Late-Onset Pompe Prevalence in Neuromuscular Medicine Academic Practices: The IPaNeMA Study. Neurol. Genet. *7*, e623.
8. Kroos, M.A., Pomponio, R.J., Hagemans, M.L., Keulemans, J.L.M., Phipps, M., DeRiso, M., Palmer, R.E., Ausems, M.G.E.M., Van der Beek, N.A.M.E., Van Diggelen, O.P., et al. (2007). Broad spectrum of Pompe disease in patients with the same c.-32-13T->G haplotype. Neurology *68*, 110–115.
9. Kohler, L., Puertollano, R., and Raben, N. (2018). Pompe Disease: From Basic Science to Therapy. Neurotherapeutics *15*, 928–942.
10. Nascimbeni, A.C., Fanin, M., Masiero, E., Angelini, C., and Sandri, M. (2012). The role of autophagy in the pathogenesis of glycogen storage disease type II (GSDII). Cell Death Differ. *19*, 1698–1708.
11. Rairikar, M.V., Case, L.E., Bailey, L.A., Kazi, Z.B., Desai, A.K., Berrier, K.L., Coats, J., Gandy, R., Quinones, R., and Kishnani, P.S. (2017). Insight into the phenotype of infants with Pompe disease identified by newborn screening with the common c.-32-13T>G "late-onset" GAA variant. Mol. Genet. Metabol. *122*, 99–107.
12. Sawada, T., Kido, J., and Nakamura, K. (2020). Newborn Screening for Pompe Disease. Int. J. Neonatal Screen. *6*, 31.
13. Klug, T.L., Swartz, L.B., Washburn, J., Brannen, C., and Kiesling, J.L. (2020). Lessons Learned from Pompe Disease Newborn Screening and Follow-up. Int. J. Neonatal Screen. *6*, 11.
14. Burton, B.K., Charrow, J., Hoganson, G.E., Fleischer, J., Grange, D.K., Braddock, S. R., Hitchins, L., Hickey, R., Christensen, K.M., Groepper, D., et al. (2020). Newborn Screening for Pompe Disease in Illinois: Experience with 684,290 Infants. Int. J. Neonatal Screen. *6*, 4.
15. Tang, H., Feuchtbaum, L., Sciortino, S., Matteson, J., Mathur, D., Bishop, T., and Olney, R.S. (2020). The First Year Experience of Newborn Screening for Pompe Disease in California. Int. J. Neonatal Screen. *6*, 9.
16. van der Wal, E., Bergsma, A.J., van Gestel, T.J.M., In 't Groen, S.L.M., Zaehres, H., Araúzo-Bravo, M.J., Schöler, H.R., van der Ploeg, A.T., and Pijnappel, W.W.M.P. (2017). GAA Deficiency in Pompe Disease Is Alleviated by Exon Inclusion in iPSC-Derived Skeletal Muscle Cells. Mol. Ther. Nucleic Acids *7*, 101–115.
17. Dardis, A., Zanin, I., Zampieri, S., Stuani, C., Pianta, A., Romanello, M., Baralle, F.E., Bembi, B., and Buratti, E. (2014). Functional characterization of the common c.-32-13T>G mutation of GAA gene: identification of potential therapeutic agents. Nucleic Acids Res. *42*, 1291–1302.
18. van der Wal, E., Bergsma, A.J., Pijnenburg, J.M., van der Ploeg, A.T., and Pijnappel, W.W.M.P. (2017). Antisense Oligonucleotides Promote Exon Inclusion and Correct the Common c.-32-13T>G GAA Splicing Variant in Pompe Disease. Mol. Ther. Nucleic Acids *7*, 90–100.
19. Goina, E., Peruzzo, P., Bembi, B., Dardis, A., and Buratti, E. (2017). Glycogen Reduction in Myotubes of Late-Onset Pompe Disease Patients Using Antisense Technology. Mol. Ther. *25*, 2117–2128.
20. Aung-Htut, M.T., Ham, K.A., Tchan, M., Johnsen, R., Schnell, F.J., Fletcher, S., and Wilton, S.D. (2020). Splice modulating antisense oligonucleotides restore some acid-alpha-glucosidase activity in cells derived from patients with late-onset Pompe disease. Sci. Rep. *10*, 6702.
21. Roberts, T.C., Langer, R., and Wood, M.J.A. (2020). Advances in oligonucleotide drug delivery. Nat. Rev. Drug Discov. *19*, 673–694.
22. Crooke, S.T., Liang, X.H., Baker, B.F., and Crooke, R.M. (2021). Antisense technology: A review. J. Biol. Chem. *296*, 100416.
23. Burge, S., Parkinson, G.N., Hazel, P., Todd, A.K., and Neidle, S. (2006). Quadruplex DNA: sequence, topology and structure. Nucleic Acids Res. *34*, 5402–5415.
24. Aupy, P., Echevarría, L., Relizani, K., Zarrouki, F., Haeberli, A., Komisarski, M., Tensorer, T., Jouvion, G., Svinartchouk, F., Garcia, L., and Goyenvalle, A. (2020). Identifying and Avoiding tcDNA-ASO Sequence-Specific Toxicity for the Development of DMD Exon 51 Skipping Therapy. Mol. Ther. Nucleic Acids *19*, 371–383.
25. Abujarour, R., Bennett, M., Valamehr, B., Lee, T.T., Robinson, M., Robbins, D., Le, T., Lai, K., and Flynn, P. (2014). Myogenic differentiation of muscular dystrophy-specific induced pluripotent stem cells for use in drug discovery. Stem Cells Transl. Med. *3*, 149–160.
26. Moreland, R.J., Jin, X., Zhang, X.K., Decker, R.W., Albee, K.L., Lee, K.L., Cauthron, R.D., Brewer, K., Edmunds, T., and Canfield, W.M. (2005). Lysosomal acid alpha-glucosidase consists of four different peptides processed from a single chain precursor. J. Biol. Chem. *280*, 6780–6791.
27. Raben, N., Nagaraju, K., Lee, E., Kessler, P., Byrne, B., Lee, L., LaMarca, M., King, C., Ward, J., Sauer, B., and Plotz, P. (1998). Targeted disruption of the acid alpha-glucosidase gene in mice causes an illness with critical features of both infantile and adult human glycogen storage disease type II. J. Biol. Chem. *273*, 19086–19092.
28. Huang, J.Y., Kan, S.H., Sandfeld, E.K., Dalton, N.D., Rangel, A.D., Chan, Y., Davis-Turak, J., Neumann, J., and Wang, R.Y. (2020). CRISPR-Cas9 generated Pompe knock-in murine model exhibits early-onset hypertrophic cardiomyopathy and skeletal muscle weakness. Sci. Rep. *10*, 10321.
29. Bijvoet, A.G., van de Kamp, E.H., Kroos, M.A., Ding, J.H., Yang, B.Z., Visser, P., Bakker, C.E., Verbeet, M.P., Oostra, B.A., Reuser, A.J., and van der Ploeg, A.T. (1998). Generalized glycogen storage and cardiomegaly in a knockout mouse model of Pompe disease. Hum. Mol. Genet. *7*, 53–62.
30. Ficicioglu, C., Ahrens-Nicklas, R.C., Barch, J., Cuddapah, S.R., DiBoscio, B.S., DiPerna, J.C., Gordon, P.L., Henderson, N., Menello, C., Luongo, N., et al. (2020). Newborn Screening for Pompe Disease: Pennsylvania Experience. Int. J. Neonatal Screen. *6*, 89.
31. Nino, M.Y., Wijgerde, M., de Faria, D.O.S., Hoogeveen-Westerveld, M., Bergsma, A. J., Broeders, M., van der Beek, N., van den Hout, H.J.M., van der Ploeg, A.T., Verheijen, F.W., et al. (2021). Enzymatic diagnosis of Pompe disease: lessons from 28 years of experience. Eur. J. Hum. Genet. *29*, 434–446.
32. Bergsma, A.J., In 't Groen, S.L.M., van den Dorpel, J.J.A., van den Hout, H.J.M.P., van der Beek, N.A.M.E., Schoser, B., Toscano, A., Musumeci, O., Bembi, B., Dardis, A., et al. (2019). A genetic modifier of symptom onset in Pompe disease. EBioMedicine *43*, 553–561.
33. Sazani, P., Kang, S.H., Maier, M.A., Wei, C., Dillman, J., Summerton, J., Manoharan, M., and Kole, R. (2001). Nuclear antisense effects of neutral, anionic and cationic oligonucleotide analogs. Nucleic Acids Res. *29*, 3965–3974.
34. Alonso-Barroso, E., Brasil, S., Briso-Montiano, Á., Navarrete, R., Pérez-Cerdá, C., Ugarte, M., Pérez, B., Desviat, L.R., and Richard, E. (2017). Generation and characterization of a human iPSC line from a patient with propionic acidemia due to defects in the PCCA gene. Stem Cell Res. *23*, 173–177.
35. Chal, J., Oginuma, M., Al Tanoury, Z., Gobert, B., Sumara, O., Hick, A., Bousson, F., Zidouni, Y., Mursch, C., Moncuquet, P., et al. (2015). Differentiation of pluripotent stem cells to muscle fiber to model Duchenne muscular dystrophy. Nat. Biotechnol. *33*, 962–969.